Theory of Time-Dependent Transport and Levitons in Nanowires

Written by
Jakob Westerberg

Supervised by
Dr. Rubén Seoane Souto and Assoc. Prof. Martin Leijnse

Examined by
Assoc. Prof. Carina Fasth

Division of Solid State Physics
Lund University

Autumn Semester 2020

Abstract

An interesting type of quasi-particles in solid-state materials are the so-called levitons. These are single-electron excitations above the Fermi-level that do not produce any hole states when carrying an integer multiple of the elementary charge. Levitons are produced when a quantum conductor is subjected to a time-dependent voltage pulse with a Lorentzian shape. The parameters of the voltage pulse determine the amount of charge carried by a leviton, meaning that single-electron excitations can be generated without the need for advanced nanofabrication. This makes levitons interesting for potential use in experiments and nanoelectronic devices involving single electrons.

In this thesis, I simulate the transport of levitons through one-dimension tight-binding chains. The tight-binding chains consist of a scattering region with one or two barriers, connected to leads at both ends. The goal of these simulations is to study how the properties of a leviton, in particular its shape and the amount of charge transported through the system, is affected by quantum tunnelling through the barriers. The simulations are done using a Python package called Tkwant, aimed at calculating time-dependent transport through quantum systems. The levitons are generated by applying a time-dependent voltage pulse to the left lead of the system. The results are presented as the expectation values of the current, calculated after the scattering region. The amount of charge transported is then obtained by integrating the current with respect to time. Since the expectation value of the current is proportional to the absolute value squared of the wave function, the shape of the current corresponds to the shape of the absolute value squared of the wave function. The shape of the current after the scattering region is determined by fitting a Lorentzian function (or a sum of Lorentzian functions in the case of two barriers) to the result. This shows whether the transmitted part of the wave function still has a Lorentzian shape, and if so, how the parameters of the Lorentzian have changed compared to before entering the scattering region.

The results of the simulations show that a leviton do seem to retain its shape after the tunnelling events and that the amount of charge transported through the system decrease exponentially with increased barrier height. When the barriers are much higher in energy than the leviton, the parameters of the Lorentzian curve are virtually unchanged by the tunnelling. This is likely because all energy components of the leviton transmit through the barriers with a similar probability. When the barrier height is at an energy comparable to that of the leviton, a narrowing of the Lorentzian is observed, probably due to a more prominent difference in transmittance between the high and low energy components of the leviton.

Contents

Acknowledgements

I want to say a warm thank you to my supervisors, Rubén and Martin, for giving me the opportunity to do this project and for all the help and support you have offered me along the way. I have learnt a lot from writing this thesis, both in terms of physics and in terms of pursuing a project this large. I am very grateful for that. I also want to thank the rest of the research group for making me feel welcome and included from day one. You have made my time here very pleasant.

1 Introduction

In 1900, Max Plack postulated, as a solution to the problem now known as the ultraviolet catastrophe, that the energy emitted and absorbed by a black-body radiator is quantized in discrete energy packages. Five years later, Albert Einstein generalized this idea by proposing that it is not only black-body radiation that is quantized but the energy of every electromagnetic field [1]. These ideas sowed the seed for what would later become the field of quantum mechanics. The theory of quantum mechanics proved to be immensely successful at describing the world at the smallest scales and was greatly developed throughout the last century. With this new understanding of nature at the atomic scale, the field of solid-state physics emerged in the 1940s as a way of describing the properties of solid materials from the quantum mechanical behaviour of electrons, atoms and light [2].

The advances in solid-state physics were accompanied by the rise of the semiconductor industry, making it possible to manufacture microscopic (and later nanoscopic) electrical devices which utilised the unique properties of solid-state materials [3]. These devices, perhaps most notably the transistor, allow for the creation of complex digital integrated circuits that are both orders of magnitude more powerful than their analogue counterparts, while at the same time being cheaper to produce and less power consuming [4]. The scientific development of solid-state physics made the digital revolution possible, gave us cheaper, more efficient light sources in the form of LEDs, and lead to the creation of accurate, reliable and cost-efficient sensors for measuring a variety of quantities [3]. It is hard to overstate the importance of this field to modern society, and so, it is perhaps not surprising that much research still focuses on understanding solid materials and their properties at the micro- and nanoscopic level. However, the solid-state devices of today are still made up of large numbers of atoms and electrons and do not utilise the true quantum nature of materials at the smallest scale. Taking advantage of these quantum properties could lead to novel devices and scientific discoveries that pave the way for new and emerging sub-fields of solid-state physics and electronics [5].

One such sub-field is quantum electronics, which has matured to the point where researchers are now looking at techniques to generate, transport, and detect single electrons [6][7]. This has opened up the possibility for experimental research on what is called electron quantum optics [8][9]. Electron quantum optics is the study of single electrons in ballistic quantum conductors. The premises for this field is that many of the experiments carried out using single photons should also have single electron analogues [10]. The fabrication techniques for nanoelectronic devices are developed enough to produce the equivalent of optical components for electrons in solid-state materials, such as interferometers, waveguides and beam splitters [11]. Research in this field is dependent on the generation of single electrons [10]. A potentially promising alternative to achieve this is with the use of single-electron excitations above the Fermi sea in metals. Unlike single electrons, these are quasiparticles in solid-state systems, achieved by manipulating metals or semiconductors via voltage pulses to produce an excited state behaving as a single electron [6].

Single-electron sources are important in many fields. For example, the field of quantum computing, in which single-electron sources could be a way of implementing so-called flying qubits [6]. The idea is to use coherent electron pulses to both encode and transport information between different parts of the computer. Many of the quantum computer architectures researched today rely on spatially localized states [12]. The information then has to be read from where it is being stored and communicated to other parts of the computer. The concept of flying qubits could integrate all of these steps into one single process. To do this, it is necessary to have very precise control at the single electron level. Flying qubits would also need to be coherent over long travel distances so that information is not lost when communicated between different parts of the computer.

In 1996, Leonid Levitov and colleagues theoretically showed that a metal excited by a Lorentzian-shaped voltage pulse produces a coherent excitation above the Fermi sea [13]. This quasiparticle was given the name leviton and has the special property that it minimizes noise compared to excitations generated

by voltage pulses with different profiles. A leviton can carry any amount of charge, even fractions of the elementary charge, depending on the amplitude and width of the voltage pulse used to create it. A rather amazing feature of the leviton is that when it carries an integer multiple of the elementary charge, no hole states are created [14]. For this reason, a leviton carrying one elementary charge behaves like a single electron excited above the Fermi sea.

In 2013, a group of experimentalists succeeded in creating and measuring levitons for the first time [15]. In their experiment, they applied voltage pulses to a two-dimensional electron gas. The resulting excitations were split into two parts using a quantum point contact, acting as a beam splitter. The two parts of each excitation were then filtered through circuitry to extract the current noise. The current noise from each part of the excitation was converted to a voltage signal after which the cross-correlation between the signals was calculated. Generally, when a periodic voltage is applied to a conductor, a number of neutral excitations are created in addition to the generated current pulse [14]. If N_e is the total number of excited electrons, and n is the charge carried by the current pulse, $N_h = N_e - n$ hole states will be created. For the periodic voltages used in the experiment in ref. [15], the minimum amount of current noise is $S_I^0 = nS_0 = 4e^2nfD(1-D)$, where e is the elementary charge, f is the frequency of the periodic voltage, and D is the transmission probability for the quantum point contact. With the generation of neutral excitations the total current noise becomes $S_I = 4e^2fD(1-D)(N_e + N_h)$ [15]. The researchers compared the minimal expected current noise to the total measured current noise to calculate the number of neutral excitations, $(S_I - S_I^0)/S_0 = N_e + N_h - n = \Delta N_{eh}$. If no neutral excitations are create $N_e = n$, and so $\Delta N_{eh} = 0$.

The researchers performed the experiment for three different voltage profiles; square wave, sine wave, and Lorentzian-shaped. What they found was that the Lorentzian-shaped voltage pulses produced the least amount of neutral excitations. They also found that when a leviton carries an integer amount of charge no neutral excitations were created, verifying the theoretical work done by Levitov and colleagues. The main result of their paper is shown in figure (1.1).

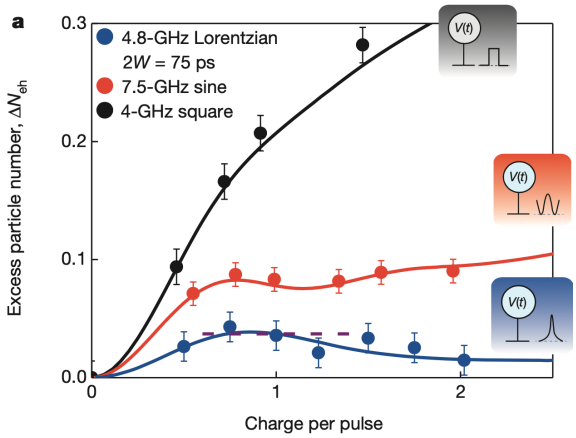

Figure 1.1: Figure is taken from ref. [15]. The y-axis shows the number of neutral excitations created. The x-axis shows the amount of charge carried by the current pulse. The dashed purple line shows the thermal noise for both a Lorentzian pulse and a sine wave generating a pulse containing one elementary charge. In that situation, the thermal noise dominates the measurement for the Lorentzian pulse while the sine wave exhibit noise above the thermal contribution.

As can be seen in figure (1.1), the Lorentzian pulse always minimizes noise compared to the sine wave and the square wave, independent of the charge carried. In the case when the current pulse carries an integer multiple of the elementary charge the only noise contribution comes from thermal noise, indicating a minimal number of neutral excitations. This is in agreement with the theoretical work done by Levitov and colleagues and verifies that levitons can be created.

Compared to other approaches to single-electron sources, creating levitons is fairly easy to do as it does not require any special nanofabrication [6]. The most difficult part about their creation is the voltage pulse. The pulse needs to be very short for the leviton to have good temporal localization. As seen in the legends in figure (1.1), each Lorentzian pulse has a width of 75 ps with a repetition frequency of 4.8 GHz. For the potential use-case of levitons as qubits in quantum computers, where the qubit state is encoded as the charge or the spin of the leviton [6], it is desirable to have each pulse as short as possible and the frequency of pulses as high as possible since this determines the speed of computation. The amplitude of the voltage pulse also needs to be controlled to a high degree of precision to have good control over the amount of charge carried by the current pulse. For a train of Lorentzian pulses with repetition frequency f, where each pulse creates an excitation with charge q, the amplitude of the voltage pulse becomes qhf/e, where h is Planck's constant and e is the elementary charge [15]. For one elementary charge to be transported through the system described in ref. [15], the voltage pulses must have an amplitude of 20 μV. Increasing the amplitude by just 10 μV leads to pulses carrying $1.5e$ instead of $1e$. Therefore, accurate control over the voltage pulses are important to generate precise excitations.

In this thesis, I simulate the generation and transport of levitons in a one-dimensional tight-binding chain, using a software package called Tkwant. I study the transmissions and reflections of levitons through finite potential barriers to understand the transport of levitons through heterostructures consisting of two materials. Ultimately, the goal of this thesis is to make a simple nanowire model and study how a leviton is transported through such a system. I examine how the shape of a leviton is affected by transmission through barriers and how the tunnelling probably of levitons is affected by barrier height.

2 Theoretical Background

2.1 Scattering Theory

To calculate time-dependent observables, such as current, in a quantum system, one first needs to calculate the electron transport properties of that system. There are several formalisms in which to do this, for example, Green's functions and master equations [16]. In this thesis, however, I will use the scattering formalism developed by Landauer and Büttiker. The primary interest of scattering theory is to calculate electron transport through a system consisting of a conducting mesoscopic scattering region connected to macroscopic leads [17]. Because the leads in such a system are so much larger than the scattering region, they can be thought of as infinite electronic reservoirs. It makes it possible to apply an important approximation to the scattering problems considered under this formalism, namely, that the leads occupied density of states does not change no matter how many electrons enter into the scattering region from a lead, or how many electrons exit out of the scattering region into a lead [17].

For this thesis, it is of interest to calculate the current in such a system. In the Landauer-Büttiker formalism, one starts by introducing a basis of plane waves in the leads. Any incoming or outgoing wave can be expressed as a linear combination of wave functions that constitutes an orthonormal basis

$$\Psi^{in} = \sum_{\alpha}^{N} a_\alpha \psi_\alpha^{in}, \tag{2.1}$$

$$\Psi^{out} = \sum_{\beta}^{N} b_\beta \psi_\beta^{out}, \tag{2.2}$$

where N is the number of basis states, Ψ^{in} is the unscattered wave function, and Ψ^{out} is the scattered wave function. Ψ^{out} contains information about which parts of Ψ^{in} are transmitted and which parts are reflected. The problem of describing an outgoing wave given some incoming wave becomes a matter of calculating how the basis wave functions are transmitted and reflected in the scattering region. To do this it is necessary to find a scattering matrix, $\hat{S}$, such that

$$\hat{b} = \hat{S}\hat{a}, \tag{2.3}$$

where

$$\hat{a} = \begin{pmatrix} a_1 \\ a_2 \\ \vdots \\ a_N \end{pmatrix}, \quad \hat{b} = \begin{pmatrix} b_1 \\ b_2 \\ \vdots \\ b_N \end{pmatrix}. \tag{2.4}$$

The scattering matrix contains information about how some incoming wave reflects and transmits in the scattering region. One requires Ψ^{in} and Ψ^{out} to be normalized, so that

$$\int dx |\Psi^{in}|^2 = \int dx |\Psi^{out}|^2 = 1, \tag{2.5}$$

Inserting equation (2.1) in (2.5) gives

$$\int dx \sum_{\alpha} a_\alpha \psi_\alpha^{in} \sum_{\alpha'} a_{\alpha'}^* \psi_{\alpha'}^{*\,in} = \sum_{\alpha\alpha'} a_\alpha a_{\alpha'}^* \int dx \; \psi_\alpha^{in} \psi_{\alpha'}^{*\,in} = \sum_{\alpha} |a_\alpha|^2 = 1. \tag{2.6}$$

where the fact that the set $\{\psi_\alpha\}$ forms an orthonormal basis is used to replace the integral with a Kronecker delta. The vector representation of the coefficients in equation (2.1) gives

$$\sum_\alpha |\alpha|^2 = \hat{a}^\dagger \hat{a} = 1. \tag{2.7}$$

The same calculations can be done for Ψ^{out}, giving equivalent relations for the coefficients in equation (2.2). Now, using equation (2.7), together with (2.3) and its Hermitian conjugate, one get

$$\hat{b}^\dagger \hat{b} = \hat{a}^\dagger \hat{a} = \hat{a}^\dagger \hat{S}^\dagger \hat{S} \hat{a} = 1 \quad \Rightarrow \quad \hat{S}^\dagger \hat{S} = \hat{I}, \tag{2.8}$$

where $\hat{I}$ is the identity matrix. This proves that $\hat{S}$ is unitary, which is what one would demand from a physical point of view as well because the unitary property means that particle number is conserved during scattering.

In the absence of a magnetic field, a scattering state $\Psi(t)$ transforms under time reversal as [18]

$$\hat{\Theta}\Psi(t) = \Psi^*(-t), \tag{2.9}$$

where $\hat{\Theta}$ is the time reversal operator. Inserting equation (2.2) in the above equation gives

$$\hat{\Theta}\Psi^{out}(t) = \Psi^{*\ out}(-t) = \sum_\beta b^*_\beta \psi^{*\ out}_\beta(-t). \tag{2.10}$$

With a change of variables, $\psi^{*\ out}_\beta(-t) \to \tilde{\psi}^{in}_\beta(t')$ (and a corresponding change for $\psi^{*\ in}_\alpha(-t)$), the time reversed states can be inserted in to equation (2.3) leading to [17]

$$\hat{a}^* = \hat{S}\hat{b}^*. \tag{2.11}$$

In essence, the time reversal operator has the effect of interchanging the sets of outgoing and incoming scattering states, while also complex conjugating the coefficients. "Running the clock backwards" should be equivalent to interchanging the sets of scattering states, with a change of sign for all complex-valued phases. Multiplying the equation above with $\hat{S}^\dagger$ from the left results in

$$\hat{S}^\dagger \hat{a}^* = \hat{S}^\dagger \hat{S} \hat{b}^* \implies (\hat{b}^*)^* = (\hat{S}^\dagger \hat{a}^*)^* \implies \hat{b} = \hat{S}^T \hat{a}. \tag{2.12}$$

By comparison with equation (2.3) one can see that $\hat{S} = \hat{S}^T$, i.e. the scattering matrix is symmetric. From this it can be concluded that the scattering matrix has the block matrix form

$$\hat{S} = \begin{pmatrix} R_L & T \\ T & R_R \end{pmatrix}, \tag{2.13}$$

where R_L is a submatrix describing reflection from the left lead back to the left lead, R_R is reflection from the right lead back to the right lead, and T is transmission between the leads. The absolute value squared of each element describes the probability for some specific incoming basis state to transition to some specific outgoing basis state [19]. That is, $\psi_\alpha \xrightarrow{\text{probability} = |S_{\beta\alpha}|^2} \psi_\beta$.

2.1.1 Transmission Through a Square Potential Barrier

The transmission of a free particle wavefunction, $e^{ik_1 x}$, through a square barrier is energy dependent, following the transmission function [19]

$$t = \frac{2k_1 k_2 e^{-ik_1 a}}{2k_1 k_2 \cos(k_2 a) - i(k_1^2 k_2^2)\sin(k_2 a)}, \tag{2.14}$$

where $k_1 = \sqrt{2mE/\hbar^2}$, $k_2 = \sqrt{2m(E-V_0)/\hbar^2}$. The transmission probability, T, is then given by

$$T = |t|^2. \tag{2.15}$$

Any incident wave function can be expanded in a base of free particle wave functions, and the transmission probability through a square barrier for each of those basis functions can be calculated via equation (2.15). By then transforming the wave function back to its original base, the transmission of any arbitrary wave function through a square barrier can be calculated.

2.1.2 Scattering in a Two-Barrier System

In this thesis, I will focus on one-dimensional systems with two potential barriers of equal height and width, connected to two leads. I study these systems using a software package called Tkwnat, but for the sake of theoretical understanding, I will first present a simple analytical treatment. A schematic picture of the scattering situation is shown in figure (2.1) below.

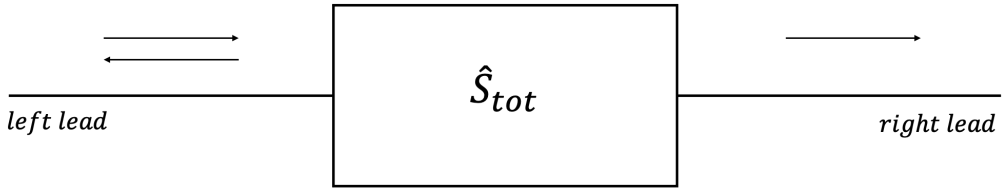

Figure 2.1: Schematic representation of the scattering region with connected in- and outgoing leads. The arrows represent in- and outgoing waves and $\hat{S}_{tot}$ is the scattering matrix for the system.

However, since the scattering region contains two barriers, the scattering situation can be broken down further into a more detailed view as shown in figure 2.2.

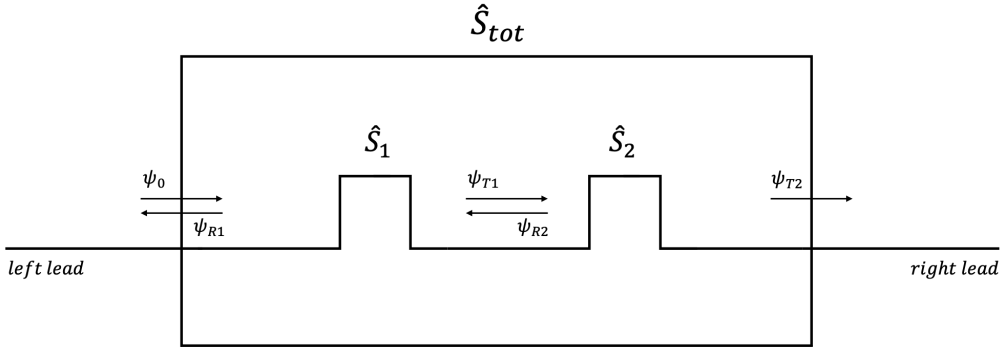

Figure 2.2: A more detailed picture of the scattering region in figure (2.1), showing the constituents of $\hat{S}_{tot}$. $\hat{S}_1$ and $\hat{S}_2$ are the scattering matrices for the two barriers. ψ_0 is the incoming wave. ψ_{T1} and ψ_{R1} are the transmitted and reflected parts of ψ_0 due to scattering at the first barrier. ψ_{T2} and ψ_{R2} are the transmitted and reflected parts of ψ_{T1} due to scattering at the second barrier.

Each barrier can be represented by its own scattering matrix, shown as $\hat{S}_1$ and $\hat{S}_2$ in the figure. The system considered here have two equal barriers, that is $\hat{S}_1 = \hat{S}_2$. A general scattering state is represented as a column vector consisting of the basis functions for both the left and the right lead,

$$\begin{pmatrix} \hat{a} \\ \hat{b} \end{pmatrix}. \tag{2.16}$$

Using the matrix in (2.13), and representing an incoming wave from the left lead as

$$\begin{pmatrix} \psi_0 \\ 0 \end{pmatrix}, \tag{2.17}$$

one can calculate the transmission to any desired order of scattering events. For the first scattering event we get

$$\begin{pmatrix} R_L & T \\ T & R_R \end{pmatrix} \begin{pmatrix} \psi_0 \\ 0 \end{pmatrix} = \begin{pmatrix} R_L\psi_0 \\ T\psi_0 \end{pmatrix} = \begin{pmatrix} R_L\psi_0 \\ 0 \end{pmatrix} + \begin{pmatrix} 0 \\ T\psi_0 \end{pmatrix}. \tag{2.18}$$

$R_L\psi_0$ is the same state as ψ_{R1} in figure (2.2). This is the part of ψ_0 that will be reflected back into the left lead and not contribute to any further scattering events. For the second scattering event we then get

$$\begin{pmatrix} R_L & T \\ T & R_R \end{pmatrix} \begin{pmatrix} 0 \\ T\psi_0 \end{pmatrix} = \begin{pmatrix} TT\psi_0 \\ R_RT\psi_0 \end{pmatrix}. \tag{2.19}$$

The doubly transmitted part, $TT\psi_0$, will enter the right lead and not return to the scattering region. Therefore, this part of the wave will not undergo any further scattering. The part of the wave that undergoes reflection at the right barrier, $R_RT\psi_0$, will take part in more scattering events, contributing to higher-order transmission through the scattering region into the right lead. The part of ψ_0 that is transmitted through the scattering region, to the right lead, is the sum of all transmissions through the right barrier.

2.2 Tight Binding Model and Second Quantization

The often difficult task of calculating quantum mechanical observables in a solid-state system with a huge number of interacting electrons can be made easier via approximative methods. In systems where the interactions between electrons are very weak, one can neglect the interactions and treat the system as if it only consists of single-particle states. Such an approximation can be made for the systems treated in this thesis. This simplifies things immensely, as it is much simpler to do calculations for the single-particle case than it is for the many-body case. One way to calculate the single-particle states is by using tight-binding approximation [20], which is the method I will use.

2.2.1 Discretizing Space

In the tight-binding approximation, the solid is discretized to a set of electronic sites. These sites can be understood as atoms or points in a larger scale discretization of the material. In this thesis, only adjacent sites are assumed to couple. The simplest system where this approximation can be applied is a material consisting of only one element where all electrons, except the valance electrons, are assumed to be tightly bound to the atoms. Then, it is the valence orbitals that make up the basis functions of the Hilbert space since all other electrons are tightly bound to the atoms in the lattice. The system wave function is a superposition of the localized basis functions [21]. In this thesis, a much larger scale discretization will be used since an atomic discretization would be computationally infeasible for a mesoscopic system.

When discretizing a crystal lattice as a set of electronic sites arranged in a chain, plane, or volume (depending on the dimensions of the system), it is convenient to label the basis states with integer indices in relation to some chosen origin site. In this formalism, the states at site x are represented using the notation $|x\rangle = |\vec{r}, \alpha\rangle$, where $\vec{r}$ is a lattice vector and α are the electronic degrees of freedom, such as spin or orbital, for the states at that site [22]. This thesis will focus on one dimensional systems in which $\vec{r} \to r = x \cdot a$, where a is the distance between sites. Further, this thesis will consider a spinless system, so the state $|x\rangle$ will represent one electronic state at site x that is either occupied by one or zero electrons. I will not consider any magnetic fields or other effects where spin plays an important role, so treating the system as spinless will not impact the results in any significant way.

The Hamiltonians in this thesis are described in the formalism of second quantization. Second quantization only considers which single-particle states are occupied, and which ones are not. A many-body state in this formalism is described by the notation

$$|\Psi\rangle = |n_{\lambda_1}, n_{\lambda_2}, ..., n_{\lambda_i}\rangle\,, \tag{2.20}$$

where λ_i represents a single-particle state and n_{λ_i} is the number of particles occupying that state [23]. For fermions, $n_{\lambda_i} = 1$ or 0 because of the Pauli exclusion principle and the fact that I consider the spinless case. In my tight-binding approximation, I do not consider many-body interactions. Therefore, when calculating a single-particle state, the system can be treated as if all states λ_i are unoccupied, except for one. The different many-body states are related to each other via the creation and annihilation operators, $\hat{c}^\dagger_{\lambda_i}$ and $\hat{c}_{\lambda_i}$, with the following properties [20]

$$\hat{c}^\dagger_{\lambda_i}\,|n_{\lambda_j}\rangle = \delta_{ij}\begin{cases} 0, & \text{for } n_{\lambda_j} = 1 \\ |1\rangle\,, & \text{for } n_{\lambda_j} = 0 \end{cases}, \tag{2.21}$$

$$\hat{c}_{\lambda_i}\,|n_{\lambda_j}\rangle = \delta_{ij}\begin{cases} |0\rangle\,, & \text{for } n_{\lambda_j} = 1 \\ 0, & \text{for } n_{\lambda_j} = 0 \end{cases}. \tag{2.22}$$

In essence, the effect of $\hat{c}^\dagger_{\lambda_i}$ is to create a particle if the state is empty and the effect of $\hat{c}_{\lambda_i}$ is to destroy a particle if the state is occupied. The product of these two operators is an operator that measures the number of particles,

$$\hat{n}_{\lambda_i} = \hat{c}^\dagger_{\lambda_i}\hat{c}_{\lambda_i}. \tag{2.23}$$

From equations (2.21) and (2.22) one get that $\hat{n}_{\lambda_i}\,|1\rangle = |1\rangle$ and $\hat{n}_{\lambda_i}\,|0\rangle = 0$. The expectation value of the particle number operator then becomes

$$\langle\hat{n}_{\lambda_i}\rangle = \langle n_{\lambda_i}|\,\hat{c_{\lambda_i}}^\dagger\hat{c_{\lambda_i}}\,|n_{\lambda_i}\rangle = \begin{cases} 1, & \text{for } n_{\lambda_i} = 1 \\ 0, & \text{for } n_{\lambda_i} = 0 \end{cases}. \tag{2.24}$$

Equation (2.23) will come in handy when deriving the current operator in second quantization. If the states λ_i include a positional component, the propagation of an electron in this formalism can be described by destroying the electron at its current site and creating an electron at a neighbouring site. This makes tight binding and second quantization very suited to use together.

2.2.2 Discretizing the Hamiltonian

With a discretization of space in place, one must also discretize all operators containing a position component. The free particle Hamiltonian reads

$$\hat{H}_0 = -\frac{\hbar^2}{2m}\nabla^2. \tag{2.25}$$

Discretizing this Hamiltonian becomes a matter of discretizing the second-order spatial derivatives. This can be done using the central difference approach [24]. In one dimension, which is what this thesis considers, the discretized differential operator then takes the following form

$$\frac{\partial^2}{\partial x^2} \to \sum_{i=0}^{N} \frac{|i+1\rangle\langle i| - 2\,|i\rangle\langle i| + |i-1\rangle\langle i|}{a^2}, \tag{2.26}$$

where a is the distance between sites in the used discretization and N is the number of sites in the system [25]. For a spinless one-dimensional system, the matrix representation of the Hamiltonian then becomes

$$\hat{H}_0 = \begin{pmatrix} 2t & -t & 0 & \dots & 0 \\ -t & 2t & -t & & \vdots \\ 0 & -t & 2t & \ddots & 0 \\ \vdots & & \ddots & \ddots & -t \\ 0 & \dots & 0 & -t & 2t \end{pmatrix}, \tag{2.27}$$

with $t = -\frac{\hbar^2}{2ma^2}$. The diagonal elements of this matrix are the onsite energies at each site in the system and the off-diagonal elements are the hopping energies between neighbouring sites. The fact that the matrix has a tridiagonal form reflects the fact that electrons are only allowed to jump between neighbouring sites.

A potential term of the form

$$\hat{v}(x) = \begin{cases} v_0, & \text{for } x_0 \leq x \leq x_1 \\ 0, & \text{otherwise} \end{cases}, \tag{2.28}$$

where x_0 and x_1 are the boundries of the region affected by the potential, is straight forward to add to the Haliltonian in equation (2.27) using this discretization. The discretized potential becomes

$$\hat{v}(x) \to v_0 \left|i\right\rangle \left\langle i\right|, \text{ for } i_0 \leq i \leq i_1, \tag{2.29}$$

where i_0 and i_1 are the indices of the boundary sites for the potential. The resulting matrix form of $\hat{v}$ will then be a diagonal matrix where the diagonal element i is v_0 if $i_0 \leq i \leq i_1$ and 0 otherwise. The matrix form of the potential contains no hopping terms, since $\langle i|j\rangle = \delta_{ij}$. With the inclution of the potential, the Hamiltonian for the system chagnes as

$$\hat{H} = \hat{H}_0 + \hat{v}. \tag{2.30}$$

Later in this thesis, I will use potentials of this form as a way of implementing potential barriers in my models of one-dimensional systems.

If spin were to be included in the model, the Hamiltonian would change as

$$\hat{H}_{spinfull} = \hat{H} \cdot \sigma_0, \tag{2.31}$$

where σ_0 is the 2×2 identity matrix, and the multiplication here is element-wise multiplication, not matrix multiplication. Multiplying each element of the spinless Hamiltonian with σ_0 is necessary to account for the two degenerate electron states at each site. This would lead to a doubling of the current since the system could then accommodate two electrons at each energy.

In a tight-binding model with spinless electrons, a one-dimensional system with one orbital on each site will only contain one band. By calculating the energy spectrum of the discretized Hamiltonian, one can show that the band will have the following shape in the first Brillouin zone

$$E = 2t - 2t \cdot \cos(ak), \tag{2.32}$$

where E is the energy and k is the wave vector [26]. The band has a translational invariance in reciprocal space, $k = k + 2\pi/a$. Using the Einstein-Planck relation, $E = \hbar\omega$, the Fermi velocity, v_F, can then be calculated as [19]

$$v_F = \frac{\partial \omega}{\partial k} = \frac{1}{\hbar}\frac{\partial E}{\partial k} = \frac{2at}{\hbar}\sin(ak). \tag{2.33}$$

If the tight-binding chain were expanded to a two-dimensional system, by stacking one-dimensional chains in the second dimension, the system would gain one new band per chain added in the second dimension, and the size of the Hamiltonian would grow quadratically.

2.2.3 Expectation Value of the Current Operator

The main results of this thesis require calculating the expectation value of the current through the systems that I model. The analytical expression for the current can be derived using the particle number operator, defined in equation (2.23). The current, $\hat{I}$, passing through a site i_0 is the change in the number of particles at that site (multiplied by the elementary charge). That is,

$$\hat{I} = e\frac{\partial \hat{n}_{i_0}}{\partial t} = e\frac{\partial \hat{c}^\dagger_{i_0}\hat{c}_{i_0}}{\partial t} = e\left(\frac{\partial \hat{c}^\dagger_{i_0}}{\partial t}\hat{c}_{i_0} + \hat{c}^\dagger_{i_0}\frac{\partial \hat{c}_{i_0}}{\partial t}\right). \tag{2.34}$$

The derivatives of the creation and annihilation operators are straight forward to calculate using the Heisenberg picture and assuming a Hamiltonian of the form $\hat{H} = \sum_{i,j} H_{ij}\hat{c}^\dagger_i\hat{c}_j$ (the matrix representation of this Hamiltonian is shown in equation (2.27)),

$$\frac{\partial \hat{c}^\dagger_{i_0}}{\partial t} = \frac{i}{\hbar}\sum_k H_{i_0k}\hat{c}^\dagger_k, \tag{2.35}$$

$$\frac{\partial \hat{c}_{i_0}}{\partial t} = -\frac{i}{\hbar}\sum_k H_{i_0k}\hat{c}_k, \tag{2.36}$$

where k is an index running over every site in the system and the constant i is the imaginary unit. Putting equation (2.35) and (2.36) into (2.34) then yields

$$\hat{I} = i\frac{e}{\hbar}\left(\sum_k H_{i_0k}\hat{c}^\dagger_k\hat{c}_{i_0} - \sum_k H_{i_0k}\hat{c}^\dagger_{i_0}\hat{c}_k\right). \tag{2.37}$$

Since I only consider nearest neighbour hoppings, all elements of the Hamiltonian, H_{i_0k}, are zero except for when $k = i_0 \pm 1$. The current from site i_0 to site i_0+1 (using the fact that $H_{i_0i_0+1} = -t$) then becomes

$$\hat{I} = -i\frac{et}{\hbar}\left(\hat{c}^\dagger_{i_0+1}\hat{c}_{i_0} - \hat{c}^\dagger_{i_0}\hat{c}_{i_0+1}\right). \tag{2.38}$$

Finally, the expectation value of the current is calculated as

$$\langle\hat{I}\rangle = -i\frac{et}{\hbar}\left(\langle\hat{c}^\dagger_{i_0+1}\hat{c}_{i_0}\rangle - \langle\hat{c}^\dagger_{i_0}\hat{c}_{i_0+1}\rangle\right). \tag{2.39}$$

2.3 Levitons

Many types of quasiparticles have been discovered in the field of solid-state physics [19]. One such particle is the so-called leviton, first described by Levitov and colleagues in 1996 [13]. They found that a conducting quantum mechanical system excited by a voltage pulse, whose shape is the sum of Lorentzian-shaped pulses, minimizes the quantum noise from the current, particularly when the pulse carries an integer amount of charge.

The general form of the voltage pulses required to generate Levitons are

$$V(t) = \frac{h}{\pi e}\sum_{j=1}^{n} \pm\frac{W_j}{(t-\tau_0^j)^2 + W_j^2}, \quad W_j > 0. \tag{2.40}$$

W_j is the width of pulse j, t is time, and τ_0^j is the time at which the pulse has reached its maximum value. When the electrons in a conductor are subjected to a time-dependent bias voltage, $V(t)$, their wave functions are shifted by a time-dependent phase given by [15]

$$\phi(t) = \frac{e}{\hbar}\int_{-\infty}^{t} V(t')dt', \tag{2.41}$$

where $\phi(t)$ is the phase acquired. The total charge carried by a pulse is calculated as [15]

$$Q = \frac{e}{2\pi}\left[\lim_{t\to\infty}\phi(t) - \lim_{t\to-\infty}\phi(t)\right] = \frac{e}{2\pi}\Delta\phi. \tag{2.42}$$

As can be seen from the equation above, Q becomes an integer multiple of the elementary charge precisely when $\Delta\phi = 2\pi$. What is also interesting to note here is that $\Delta\phi$ can be tuned to have whatever value one wishes depending on which multiplicative constants are chosen for $V(t)$, so a leviton can carry a fractional charge as well.

3 Method

3.1 Tkwant

3.1.1 Creating a System

To model my system, and carry out the simulations, I have used a Python package called Tkwant which is an extension of the Kwant Python package [24]. Kwant is aimed at calculating quantum observables in a stationary system using tight-binding approximation. Tkwant builds on this by allowing the Hamiltonian to be time-dependent. The process of modelling a system in Tkwant starts with defining the geometry. Both Kwant and Tkwant describe the systems in terms of tight-binding models, so the user must first define the lattice. Then the shape of the system can be defined by iterating over lattice points, using for example a for-loop, or by defining a function that takes a lattice point as its argument and returns a boolean value based on whether the given lattice point belongs to the system or not [22]. The latter way allows Tkwant to automatically find which points belong to the system, and which ones do not. Tkwant allows system geometries in any arbitrary number of dimensions, even greater than three, but the scope of this thesis is limited to one-dimensional systems. The user defines an onsite energy for every site in the system and a hopping energy between all neighbouring sites. The onsite energies are the diagonal elements of equation (2.27), and the hopping energies are the off-diagonal elements. Because I only consider nearest neighbour hoppings, all off-diagonal entries in (2.27) are zero except for the ± 1 diagonals.

In Tkwant one can create isolated systems. However, for many applications, it is of interest to study open systems, connected via leads to some outside reservoirs. This is done by defining leads in much the same ways that the system itself was defined [24]. Each lead must be created with a lattice and a geometry. The difference compared to defining the main system is that the leads are considered infinite, so only one unit cell of the lattice is needed and Tkwant builds up the lead by repeating that unit infinitely. Once the leads are defined, various parameters such as Fermi-level and temperature can be set. There is no direct support in Tkwant to add a time-dependent bias voltage to the leads, but this can be worked around by doing a gauge transformation of the voltage to a time-dependent phase, according to equation (2.41). The time-dependent phase can then be added to the hopping between a lead and the system. Practically, Tkwant introduces this time-dependent hopping element by adding a new site, that is inaccessible to the user, between the lead and the scattering region. The parameters for this newly added site are the same as for the lead. The hopping between the site and the system carries the phase term.

3.1.2 Calculations in Tkwant

The constituents of a Tkwant system are the scattering region and leads attached to that scattering region, so the general form for a Hamiltonian in Tkwant reads

$$\hat{H}(t) = \hat{H}^s(t) + \sum_l \hat{H}^l + \sum_l \hat{H}^{sl}(t), \tag{3.1}$$

where $\hat{H}^s(t)$ is the Hamiltonian for the scattering region, $\hat{H}^l$ is the Hamiltonian for lead $l = L,\ R$ and $\hat{H}^{sl}(t)$ is the Hamiltonian for the coupling between lead l and the scattering region [24]. Each term of the total Hamiltonian is defined in terms of the creation and annihilation operators in second quantization. The general form for each term of the Hamiltonian is as follows

$$\hat{H}(t) = \sum_{ij} H_{ij}(t)\hat{c}_i^\dagger \hat{c}_j. \tag{3.2}$$

For calculating transport in a quantum system, Tkwant uses the scattering wave formalism. This formalism was introduced in section 2.1 where incoming states are either reflected or transmitted when

encountering barriers in the scattering region, resulting in some set of outgoing scattering states. From the scattering matrix, Tkwant introduces one stationary scattering wave function per band in each lead. The time-evolution of each of these scattering states is then calculated using the time-dependent Schrödinger equation

$$i\frac{\partial}{\partial t}\psi_l(t,i,E) = \sum_j H_{ij}(t)\psi_l(t,j,E). \tag{3.3}$$

Because the energy is a continuous variable, calculating the expectation value of an observable requires solving an integral. The equation Tkwant uses to calculate the expectation value of some observable $\hat{A}$ is

$$\langle\hat{A}\rangle(t) = \sum_{ijl}\int \frac{dE}{2\pi} f_l(E)\psi_l^*(t,i,E)A_{ij}\psi_l(t,j,E), \tag{3.4}$$

where $f_l(E)$ is the Fermi-Dirac distribution for lead l.

3.1.3 Transferred Charge

One interesting quantity to calculate in the context of electron transport is how much charge has been transferred between the leads after a voltage pulse. This is calculated by integrating the current with respect to time, giving the net transferred charge. To verify that this works as expected in Tkwant, I compare the difference in charge given by the current integral to the net change of charge in a tight-binding chain. The chain has three sites and is connected to a lead at each end. I apply a time-dependent voltage to site 0 and calculated the expectation value of the particle number operator (defined in equation (2.24)) and the expectation value of the particle current (defined in equation (2.39)). For each site in the system, the difference in particle number between the start and end time is the net charge transferred to or from that site during the time interval. To verify that this gives the same result as the current integral, I integrate the current between each hopping in the scattering region, giving the net transferred charge both through the integral method and the particle number method. I choose to do this comparison for three sites because this is the minimum number of sites required to compare both methods. However, the conclusion does not depend on the size of the system and works for an arbitrary number of sites. One would expect the change in particle number at a site i, call it $\Delta\langle\hat{n}_i\rangle$, to equal the difference between the integrated current going from site $i-1$ to site i and the integrated current going from site i to site $i+1$. That is

$$\Delta\langle\hat{n}_i\rangle = \langle\hat{n}_i\rangle(t_{max}) - \langle\hat{n}_i\rangle(0) = \int_0^{t_{max}} dt[\langle\hat{I}_{i-1,\ i}\rangle(t) - \langle\hat{I}_{i,\ i+1}\rangle(t)]. \tag{3.5}$$

A schematic picture of the system in this example is shown in figure (3.1). The black sites belong to the scattering region and the white sites are part of the infinite leads. The connecting lines between the sites represent the hopping elements.

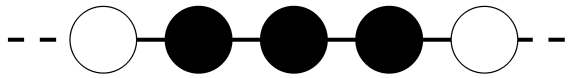

Figure 3.1: Schematic representation of the system in this example. Black sites are part of the scattering region and white sites are part of the leads. The dashed lines indicate the fact that the leads extend to infinity.

In this example system, I couple site 0 to a time-dependent gate electrode which varies the onsite energy of this site. The onsite energy of site 0 increases linearly until time $8\hbar/t$, after which it is held constant. The

resulting current and change in particle number are shown in figure (3.2). The figure shows the particle number for site 1 as a function of time, as well as the current between sites 0 - 1 and sites 1 - 2 as functions of time.

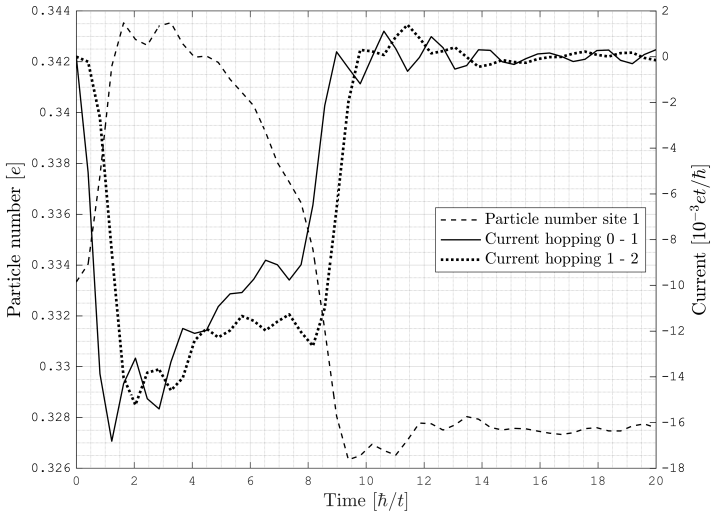

Figure 3.2: Time-dependent expectation value of the current and particle number operator.

Evaluating the difference in particle number according to equation (3.5) comes out to a net transferred charge of $0.005739e$. By instead integrating the difference in current, to and from site 1, the total transferred charge is calculated to be $0.005727e$. Therefore, the calculated net transferred charge is the same for both methods, up to numerical precision. This means that the two methods are equally valid, as expected.

3.2 Nanowire Model

The model I choose for my system is a spinless one-dimensional tight-binding chain. The system is 240 sites long with leads connected at both ends. The entire system, including the leads, is considered to be of the same material. That means that the parameters for all sites and hoppings are the same, with three exceptions. Two sites in the system, at positions 20 and 220, act as barriers in the scattering region and therefore have onsite energies higher than the other sites. The hopping element between the left lead and the system contains a time-dependent phase term to allow for a bias voltage to be applied. A schematic representation of the system is shown in figure (3.3). The black and red sites are part of the scattering region, the red sites being the barriers. The white sites are part of the leads. Lines between sites are the hopping terms, and the hopping term shown in red carries the time-dependent phase. Dashed lines represent a continuation of the system as there are too many sites to draw them all. The leads extend to infinity, indicated by non-terminated dashed lines. The x-axis shows the site indices.

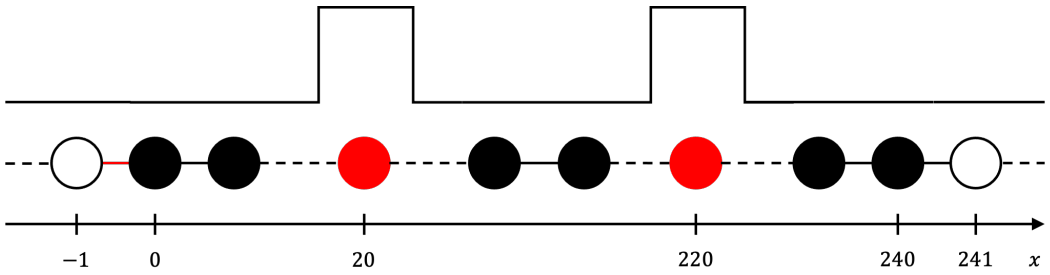

Figure 3.3: Schematic representation of the two-barrier system. The upper part shows the energy landscape and the lower part shows the corresponding tight-binding model. The x-axis shows the site indices.

With $t = -\frac{\hbar^2}{2ma^2}$ as the unit of energy, each onsite energy becomes $2t$ and each hopping energy becomes $-t$, according to equation (2.27). The system is excited by a single Lorentzian-shaped voltage pulse, defined according to equation (2.40), that gives rise to a current pulse carrying a charge of $1e$. The peak of the voltage pulse is $0.02t/e$, so in order to not have the Fermi-level too close to the energy of the pulse, I put it to $0.1t$ in both leads. A leviton is an excitation that travels on top of the Fermi-sea, so having a pulse energy that is small compared to the Feri-level means that a levtion is generated while leaving the Fermi-sea as a whole mostly undisturbed.

The Hamiltonian for my system has the following form

$$\begin{aligned}\hat{H}(t) = &\sum_{n=0,\ m=0}^{240} H^S_{nm}\ \hat{c}^\dagger_n \hat{c}_m + \sum_{n=-\infty,\ m=-\infty}^{-1} H^L_{nm}\ \hat{c}^\dagger_n \hat{c}_m + \sum_{n=241,\ m=241}^{\infty} H^R_{nm}\ \hat{c}^\dagger_n \hat{c}_m \\ &+ V_0 \hat{c}^\dagger_{20}\hat{c}_{20} + V_0 \hat{c}^\dagger_{220}\hat{c}_{220} - te^{i\phi(t)}(\hat{c}^\dagger_{-1}\hat{c}_0) - t(\hat{c}^\dagger_{240}\hat{c}_{241}) + \text{H.c.}\end{aligned} \tag{3.6}$$

The indices in the above equation represent position in the system and H_{nm} is the matrix element in the partial Hamiltonian corresponding to site or hopping nm. The scattering region starts at site 0 and ends at site 240. H^S is the Hamiltonian for the scattering region, H^L is the Hamiltonian for the left lead, and H^R is the Hamiltonian for the right lead. Each of these matrices has the form of equation (2.27). V_0 is the barrier height. I have two barriers of equal heights at sites 20 and 220, described by the terms $V_0\hat{c}^\dagger_{20}\hat{c}_{20}$ and $V_0\hat{c}^\dagger_{220}\hat{c}_{220}$. The last two terms are the hopping elements between the leads and the scattering region. The hopping element between the left lead and the scattering region carries the time-dependent phase, $e^{i\phi(t)}$.

3.3 The Process of Making the Simulations Work

When I started using Tkwant, I first tried to simulate some simple, small systems. This was a good way of learning how to write code using the Tkwant package, and how to interpret the data that I got out of the simulations. Feeling confident that I understood these simpler systems, I moved on to try and generate levitons by introducing a time-dependent voltage. What I got out of these first tries was a current that had a Lorentzian shape, as expected, but with some wired noise-like fluctuations appearing for the later time points of the simulations. My initial assumption was that I had done something wrong when defining my model. Either that the physical parameters that I had used were not realistic or that I had used the wrong functions in Tkwant. I began to methodically investigate what might have gone wrong by looking at the effects of changing just one parameter at a time. This did result in different outputs, however, which changes resulted in an improvement and which ones made things worse seemed somewhat random. For example, two different changes might improve things when tested individually, but when used together they did not improve things at all. I went back to the simpler models and tried similar changes, with good results. This process of trying to isolate the cause of the error went on for a couple of months. The most

strange thing was that everything seemed to work fine for the simpler systems but not for the systems I wanted to simulate.

I did eventually manage to find the cause of the problem. It turned out to be numerical issues. Tkwant allows the user to set the maximum tolerance for both the absolute and the relative error of the calculations. I had changed these on multiple occasions to see if they had any effects on my results, but it did not seem to make any difference. Finally, I tried putting these error tolerances to a really low value, 10^{-10}. The simulation took much longer to run than before, but the data that came out looked nice and did not show any noise for the later time points. This turned out to be the cause of the strange results and I could finally run the simulations that I wanted and get sensible data out of them. I am still not sure exactly what these error tolerances refer to. It is probably not the error of the expectation value that I calculate, since an error of 10^{-10} would be much too small to be observed. Or, perhaps, they do referer to the error of the expectation value and that error somehow accumulates as the simulation progresses. This might be why only the later time points exhibited this type of error.

4 Results

All the results presented in this section were achieved by applying a single Lorentzian shaped voltage pulse to the left lead of the system. The pulse has a width $W = 100\hbar/t$ and an amplitude of $0.02t/e$. The expectation value of the current resulting from such a pulse, in a system without barriers, is shown in figure (4.1a). The Lorentzian wave package can be expanded in a basis of free particle wave functions, as described in section 2.1. To identity the energy components of the Lorentzian pulse, I Fourier transformed it. The energy spectrum of the pulse is presented in figure (4.1b). The lowest component has an energy of $0.1t$, since the pulse rides on top of the Fermi sea.

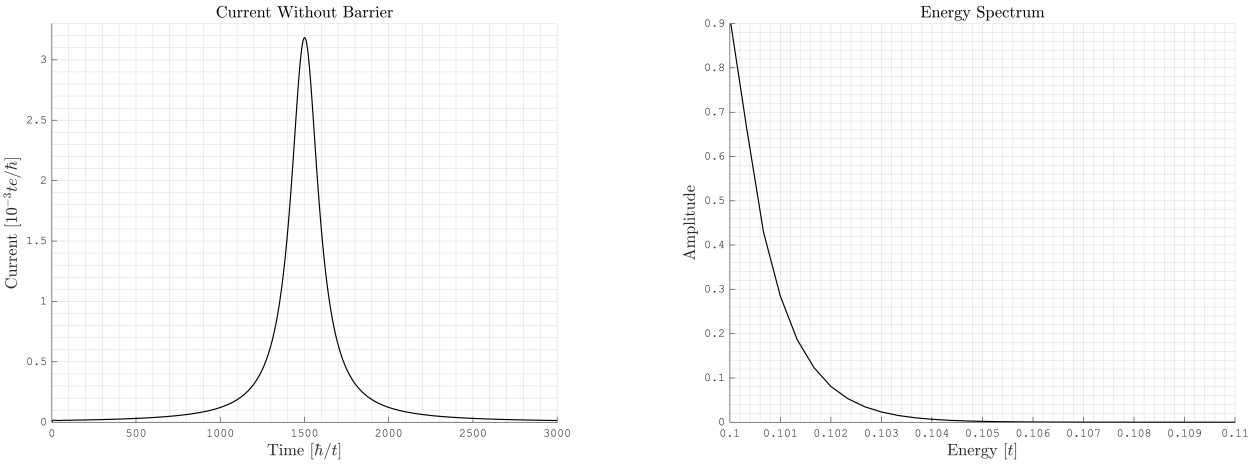

(a) (b)

Figure 4.1: (a): Expectation value of the current calculated by Tkwant for a system without barriers. (b): Energy spectrum of the current pulse shown in figure (a).

The integral of the current gives the transmitted charge, according to equation (3.5). Using this method, I calculate the total charge carried by the pulse to be $0.9566e$. From equation (2.42) one would expect the charge to equal $1e$. However, due to a finite integration time, the numerically calculated value deviates from the analytical. To show that this is the case, I redid the same calculations over a longer time interval, $[0,\ 5000\hbar/t]$. The integrated current then comes out to $0.9735e$, which is closer to the analytical value. Since I can only run the calculations over a finite time, and the tails of the Lorentzian pulse extend infinitely, there will always be an error resulting from this issue.

4.1 One Barrier

Next, I introduce one barrier to the system and calculate the expectation value of the current after the barrier. The current resulting from a barrier of height $0.4t$ above the Fermi-level is shown in figure (4.2) below. I fit a Lorentzian-shaped function to the current. This fit is also included in the figure.

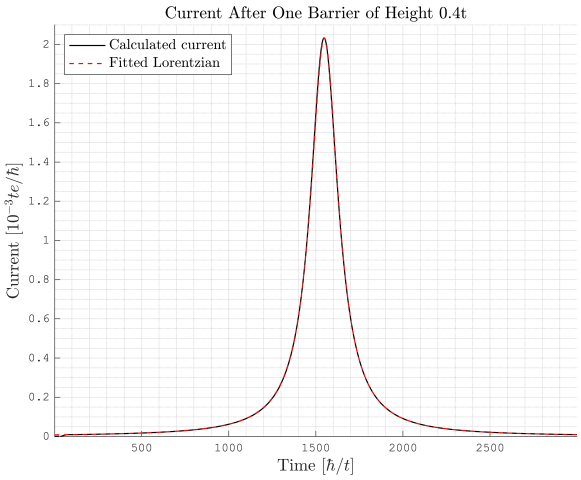

Figure 4.2: Expectation value of the current after a single-site barrier of height $0.4t$ with a fitted Lorentzian function.

The fitted Lorentzian in figure (4.2) has a root-mean-square error, RMSE, of $2.254 \cdot 10^{-6}$ compared to the calculated current. This shows that the current pulse after the barrier also has a Lorentzian shape, indicating that the leviton retains its shape after passing through a potential barrier. The width of the Lorentzian after the barrier is $97.78\hbar/t$, compared to $100\hbar/t$ before the barrier. The fact that the current has a Lorentzian shape, and that the width of the Lorentzian is relatively unchanged, means that all components of the plane wave expansion of the pulse transmit with a very similar probability. This is also what one would expect by looking at the energy spectrum of the pulse in figure (4.1b). The difference between the lowest energy component and the highest energy component is on the order of $0.01t$, one order of magnitude smaller than the barrier height. Therefore, the coefficients for all the energy components of the pulse in figure (4.1a) should decrease in a rather uniform way which has the effect of the pulse retaining its shape.

To test how the shape of the leviton changes when transmitted through a barrier with a height comparable to the energy of the pulse, I put the barrier height to $0.01t$. Compared to the other results present here, I have changed my nanowire model for this calculation so that the barrier consists of 10 sites, instead of just one site. This is because the barrier height is so low that in order for the pulse to be affected by the barrier it needs to be wider. I checked that a barrier made up of one site does not significantly affect the shape of the leviton, finding a similar result to that shown in figure (4.1a).

To determine the shape of the current, I again fit a Lorentzian function to it. The expectation value of the current calculated by Tkwant and the fitted Lorentzian are shown in figure (4.3).

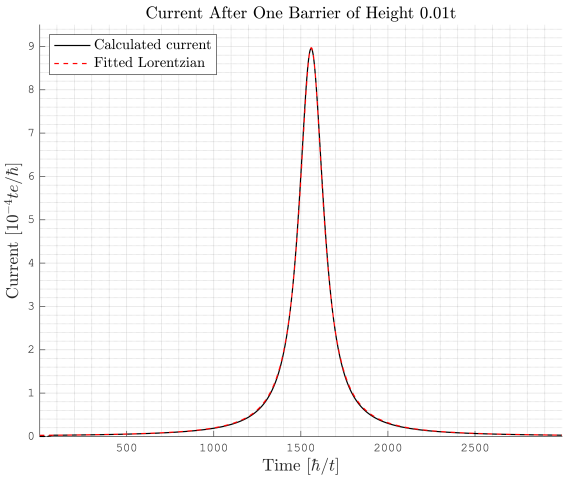

Figure 4.3: Expectation value of the current after a barrier of height $0.01t$ and width $10a$, with a fitted Lorentzian function.

As expected, the shape of the Lorentzian has changed because of the lower energy components having a lower probability of transmittance than the higher energy components. The RMSE of the fit is $1.784 \cdot 10^{-6}$, indicating that the current still has a Lorentzian shape, however the width of the fitted Lorentzian is $84.03\hbar/t$, compared to $100\hbar/t$ for the current without barriers, shown in figure (4.1a).

Although small enough to not be clearly visible, all the currents exhibit a kink at the initial time. This is the result of numerical inaccuracy in the Tkwant simulation. Tkwant assumes the system to be in equilibrium at time < 0, and considers the bias voltage to suddenly be applied at the initial simulation time. For a Lorentzian pulse, this is problematic as its tail decrease polynomially from the maximum value. Therefore, at the initial simulation time, the pulse already has some value greater than zero. This means that Tkwant sees the onset of the pulse as a step function. Consequentially, the onset of the current will also behave as a step function. For shorter pulses (smaller W-values), this problem becomes less important. However, for a shorter pulse to still carry one unit charge the maximum amplitude of the applied bias voltage must be higher. This is somewhat problematic as the applied voltage should be much smaller than the Fermi level for the simulation to remain realistic (a leviton should be a small excitation above the Fermi level and leave the Fermi sea largely undisturbed). Increasing the length of the time scale that the simulation runs over is a way to overcome this. This does however comes at the cost of longer computation times and I have therefore chosen not to do this.

4.1.1 Comparison with Analytic Expression for Transmission

The amplitudes of the pulse's energy components are proportional to the coefficients for the basis wave functions, described in equation (2.1). By multiplying the pulse's energy spectrum with the analytic expression for the transmission function in equation (2.15), and Fourier transforming it back to the time domain, I obtain the analytic tunnelling current for a square barrier. The expectation value of the current, calculated by Tkwant, and the corresponding analytical current, for a barrier of height $0.4t$ are plotted in figure (4.4). I choose the width of the square barrier to be $1a$, equal to the lattice coefficient in my tight-binding model. Since the barrier in my tight-binding system was realized by increasing the onsite energy of just one site, a width of $1a$ is the square barrier that most closely resembles my tight-binding model.

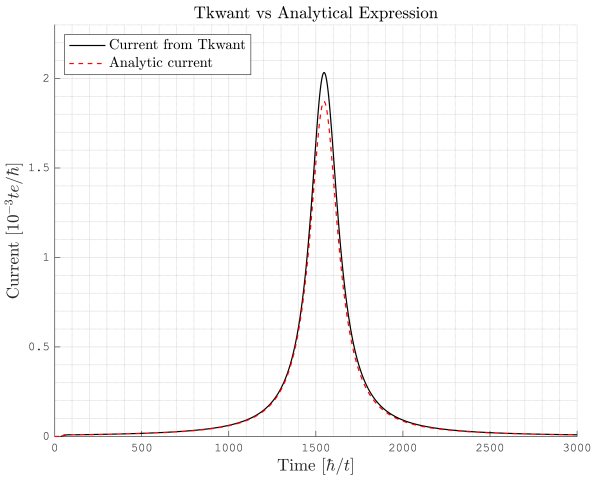

Figure 4.4: Expectation value of the current after a barrier of height $0.4t$. The black curve is the current calculated by Tkwant for the same system as in figure (4.2). The red dashed curve is the analytic tunneling current, calculated using equation (2.15), for a square barrier with height $0.4t$ and width $1a$.

The current calculated by Tkwant and the corresponding analytical tunnelling current are very similar. The shapes of the two pules are almost identical, except for the fact that the analytical current has a slightly lower peak. This could be due to a difference between the probability for hopping to a site with higher energy in my tight-binding model and the probability for transmission through a square barrier in the continuous case. The barrier in my tight-binding model is not a square barrier. However, the similarities between the two currents in figure (4.4) show that the barrier in my model is a good approximation of a square barrier.

I redid the same calculation in Tkwant and for the analytical current for potential barriers of different heights and calculated the total amount of charge transferred. The transmitted charge as a function of the barrier height is plotted in figure (4.5), as well as fitted exponential functions for the two cases.

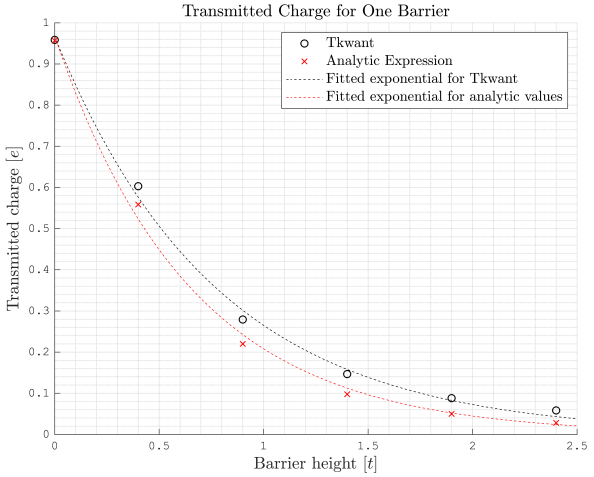

Figure 4.5: Transmitted charge as a function of barrier height. The black circles are the values calculated by Tkwant, and the red crosses are the analytical values for a square barrier. The back and red dashed curves are fitted exponential functions for the two cases.

The fitted exponential function for the charge calculated by Tkwant is $0.9668 \cdot e^{-1.294E}$, where E is the barrier height. The transmitted charge is consistently lower for the analytic case, compared to the tight-

binding model. As stated before, this is probably due to a difference in transmission probability between the barrier in my tight-binding model and a square barrier. However, the difference between the values in figure (4.5) and the difference between the currents in figure (4.4) are relatively small. Therefore, it seems reasonable to conclude that my tight-binding model is a relatively good approximation of the real system.

4.2 Two Barriers

For a system with two barriers, the current after the barriers becomes more complicated than the one studied in the previous section. The pulse is reflected and transmitted several times in the region between the two barriers. This splits the Lorentzian into different parts that exit the scattering region with a delay relative to each other. This process is depicted in figure (4.6a). Panel (1) shows the incident leviton approaching the left barrier. After the first scattering event, the leviton splits into a transmitted and a reflected part. The reflected part exits the scattering region to the left lead and does not contribute to the current in the right lead. This is shown in panel (2). The transmitted part will scatter at the right barrier, splitting the pulse again. The transmitted part from this event will enter the right lead and contribute to the current, shown in panel (3). The reflected part from scattering at the right barrier will scatter again at the left barrier, as depicted in panel (4). The amplitude of the transmitted and reflected parts will decrease polynomially with each scattering event as $(1-T)^n$, where T is the probability of transmission through a single barrier and n are the number of reflections.

The calculated expectation value of the current for the system described in section 3.2 is shown in figure (4.6b). The height of the two barriers are $0.9t$. I have also fit a sum of four Lorentzian shaped functions to this current. The result of this fit is also included in the figure. The circled number in the figure corresponds to the situation depicted in the panel with the same number in figure (4.6a).

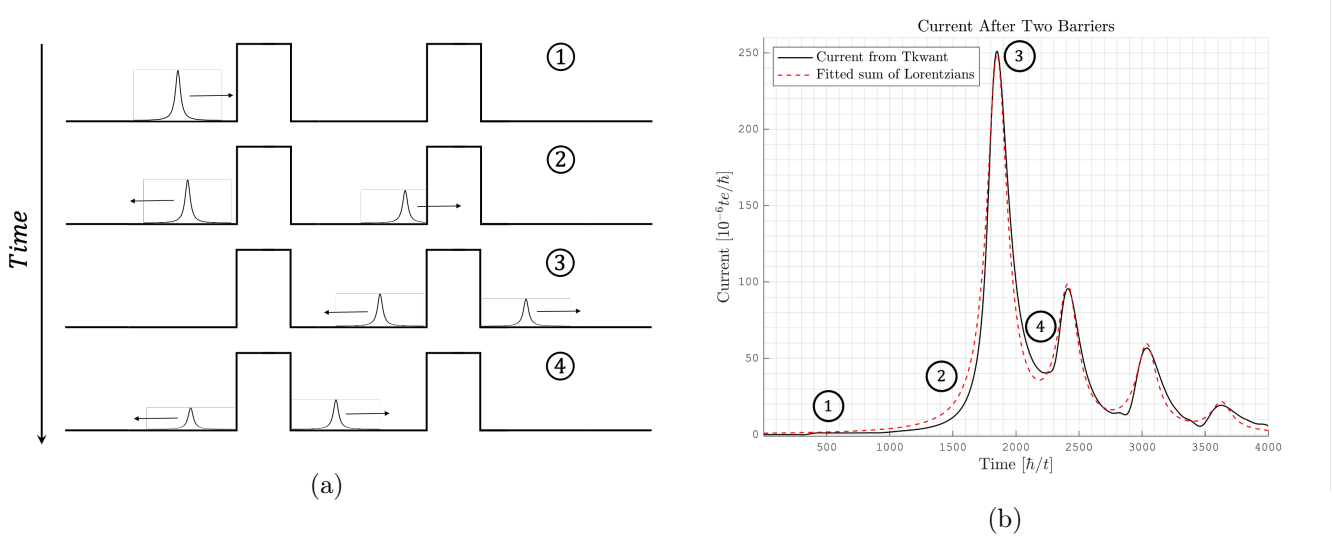

(a) (b)

Figure 4.6: (a): Schematic depiction of the scattering process in a two-barrier system. The numbers indicate the current in figure (b) that the situation in each panel gives rise to.
(b): Expectation value of the current after two barriers of height $0.9t$ with a fitted sum of four Lorentzian functions. The circled numbers indicate the corresponding situation in figure (a).

The fit in figure (4.6b) proved to be a good model for the shape of the current, with an RMSE of $7.155 \cdot 10^{-6}$. The widths of the four fitted Lorentzians are $W_1 = 99.99\hbar/t$, $W_2 = 100\hbar/t$, $W_3 = 100\hbar/t$, and $W_4 = 100\hbar/t$. As for the case of the current after one barrier, the width seems to be unaffected by the transmission through the two barriers.

The time τ_0, at which a Lorentzian has reached its peak value, for the four pulses shown in figure (4.6b)

are $\tau_0^1 = 1850\hbar/t$, $\tau_0^2 = 2410\hbar/t$, $\tau_0^3 = 3037\hbar/t$, and $\tau_0^4 = 3629\hbar/t$. This gives an average time difference between two pulses of $601.5\hbar/t$. The current was calculated for site 230, the left barrier is defined at site 20, and the right barrier is defined at site 220. The difference in travel distance between to consecutive pulses are therefore $400a$. This gives an average velocity of $0.665at/\hbar$. Calculating the Fermi velocity analytically, using equation (2.33), yields $v_F = 0.6245at/\hbar$, which is in good agreement with the value calculated using Tkwant.

In the valleys between the second and third peak, and between the third and fourth peak, some small bumps are evident in the current. I think these artefacts are due to the accumulation of numerical errors in Tkwant as the calculation progresses. To produce this plot, I had to specify the maximal allowable error in my Tkwant script to be below 10^{-10}. Without a threshold this low, the accumulated errors became so large for the later times of the calculation as to completely dominate the actual current. Lower tolerance for the error can be specified at the cost of longer computation times. However, running the calculation presented in figure (4.6b) took almost 18 hours on my laptop, so in the interest of time, I chose to not put the error threshold to a lower value.

As for the one barrier case, I redid this calculation for barriers of different heights and fitted an exponential function. The transmitted charge as a function of barrier height, as well as the exponential fit, is plotted in figure (4.7).

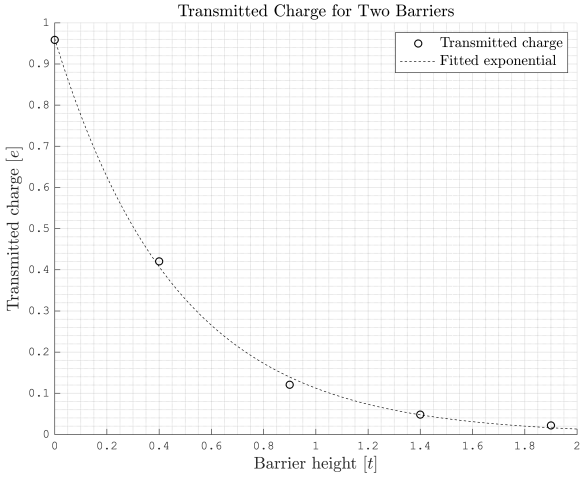

Figure 4.7: Transmitted charge as a function of barrier height. The black dashed curve is a fitted exponential function.

The fitted exponential function has the equation $0.9615 \cdot e^{-2.146E}$. The exponent here is a bit smaller than two times the exponent for the one barrier case. This is because of the process described in figure (4.6a). As the pulse reflects at the right barrier, and then again at the left barrier, several transmissions through the right barrier contribute to the current. If one only looks at the first transmission peak in the current, one would expect the exponent to be double the one barrier exponent.

5 Conclusion

In this thesis I have looked at the generation and transport of a leviton through one-dimensional tight-binding systems with both one and two potential barriers. I modelled the systems using a Python package called Tkwant, and looked at the expectation value of the current after the barriers.

From the comparison between the current calculated by Tkwant and the current calculated for transmission through a square barrier using the analytical expression, it seems that my tight-binding model is a good approximation of the analytical result for a one-dimension model with square barriers. I, therefore, regard the calculations made by Tkwant to be trustworthy and accurate numerical simulations of the corresponding continuous one-dimensional system. The results presented in figures (4.2) and (4.6b) indicate that a leviton remains as a leviton after transmission through a barrier. The results in both of these figures can be explained by the fact that the barrier height is much larger than the energies of the electron pulse. For a barrier height comparable to the pulse energy, the shape of the leviton is affected, as shown in figure (4.3). Interestingly enough though, the shape of the transmitted pulse is still Lorentzian. This is probably due to the specific properties of my tight-binding implementations of the barriers as sites with higher onsite energies. From figure (4.5), it can be seen that the transmission probability decreases exponentially with barrier height for the barriers in my system. Since the energy distribution of the Lorentzian pulse is also exponential, the effect of a barrier on the transmitted pulse's energy distribution is that of multiplying two exponential functions. The result is still an exponential function, and so the transmitted pulse still has a Lorentzian shape.

Something that I have tried to do but did not succeed with is to verify that the pulses that I have generated are levitons. For the case when a pulse carries one elementary charge, no hole states should be produced. One possible way of testing this is to attach a third lead to the system. The coupling between this third lead and the system should be weak so that it does not change the system in a significant way. If the band of the third lead is much narrower than the bands in the other two leads, the third lead could be used to probe the occupied density of states as a function of energy and time. Probing at different energies would require running the simulation multiple times with different onsite energies for the sites of the third lead. The current between the main system and the third lead should be proportional to the occupied density of states in the system. If there are no empty states below the Fermi level, then that would confirm that the excitation is a leviton. When I tried this the calculations had relatively high numerical errors which made it impossible to infer whether holes are created or not. More precise calculations would be needed to confirm if the excitations are indeed levitons.

Another question that this thesis has not answered is how long a leviton remains a leviton in a system where many-body interactions are considered. One of the assumptions made in this thesis was that many-body interactions are weak enough to be neglected. In a real system, however, the interactions between electrons do exist and would be important given long enough time scales. This would impose a limit on how long a leviton can travel in a solid-state system.

An interesting continuation of this thesis would be to simulate the transport of a leviton through an electron quantum optical component, such as a beam splitter. Doing so would give insight into how a leviton behaves in an actual electron quantum optical experiment. This thesis has only looked at the generation of levitons and their transport through square barriers. The use case as single-electron sources will require a deeper understanding of transport behaviour in more complex systems.

Bibliography

[1] G. Ireson, Physics Education **35**, 381 (2000).

[2] E. Braun, Physics Bulletin **38**, 64 (1987).

[3] J. W. Orton, *Semiconductors and the Information Revolution - Magic Crystals that made IT Happen* (Elsevier, Amsterdam, Netherlands, 2009).

[4] B. Lojek, *History of Semiconductor Engineering* (Springer-Verlag, Heidelberg, Germany, 2007).

[5] A. Laucht *et al.*, Nanotechnology **32**, 162003 (2021).

[6] C. Bäuerle *et al.*, Reports on Progress in Physics **81**, 056503 (2018).

[7] D. Ferraro *et al.*, Phys. Rev. Lett. **113**, 166403 (2014).

[8] D. C. Glattli and P. S. Roulleau, Physica Status Solidi (b) **254**, 1600650 (2017).

[9] B. Roussel *et al.*, Physica Status Solidi (b) **254**, 1600621 (2017).

[10] G. Fève *et al.*, Science **316**, 1169 (2007).

[11] Y. Ji *et al.*, Nature **422**, 415 (2003).

[12] S. Akama, *Elements of Quantum Computing. History, Theories and Engineering Applications.* (Springer, New York City, USA, 2015).

[13] L. S. Levitov, H. Lee, and G. B. Lesovik, Journal of Mathematical Physics **37**, 4845 (1996).

[14] J. Keeling, I. Klich, and L. S. Levitov, Phys. Rev. Lett. **97**, 116403 (2006).

[15] J. Dubois *et al.*, Nature **502**, 659–663 (2013).

[16] H. Bruus and K. Flensberg, *Many-body quantum theory in condensed matter physics : an introduction* (Oxford University Press, Oxford, United Kingdom, 2004).

[17] M. V. Moskalets, in *Scattering Matrix Approach to Non-Stationary Quantum Transport* (Imperial College Press, London, United Kingdom, 2011), Chap. 1, pp. 1–33.

[18] J. J. Sakurai and J. Napolitano, *Modern Quantum Mechanics* (Cambridge University Press, Cambridge, United Kingdom, 2017).

[19] J. H. Davies, *The Physics of Low-dimensional Semiconductors: An Introduction* (Cambridge University Press, Cambridge, United Kingdom, 1997).

[20] A. Šiber, American Journal of Physics **74**, 692 (2006).

[21] J. C. Slater and G. F. Koster, Phys. Rev. **94**, 1498 (1954).

[22] C. W. Groth, M. Wimmer, A. R. Akhmerov, and X. Waintal, New Journal of Physics **16**, 063065 (2014).

[23] C. Mora, *Introduction to Second Quantization*, Département de Physique, École Normale Supérieure.

[24] T. Kloss *et al.*, Tkwant: a software package for time-dependent quantum transport, 2020.

[25] A. Delploux, Bachelor's thesis, Lund University, 2020.

[26] S. H. Simon, *The Oxford Solid State Basics* (Oxford University Press, Oxford, United Kingdom, 2013).